SLC10A7, an orphan member of the SLC10 family involved in congenital disorders of glycosylation

Zoe Durin, Johanne Dubail, Aurore Layotte, Dominique Legrand, Valérie Cormier-Daire, Francois Foulquier

SLC10A7, an orphan member of the SLC10 family involved in Congenital Disorders of Glycosylation.

Zoé Durin[1], Johanne Dubail[2], Aurore Layotte[1], Dominique Legrand[1]*, Valérie Cormier-Daire[2,3]* and François Foulquier[1]* ¶

[1] Univ. Lille, CNRS, UMR 8576 - UGSF - Unité de Glycobiologie Structurale et Fonctionnelle, F-59000 Lille, France

[2] Université de Paris, INSERM UMR1163, Institut Imagine, Paris, France.

[3] Service de Génétique Clinique, Centre de Référence pour les Maladies Osseuses Constitutionnelles, AP-HP, Hôpital Necker-Enfants Malades, Paris, France.

* These authors equally contributed to this work

¶ Corresponding author

François Foulquier (francois.foulquier@univ-lille.fr), Address: Univ. Lille, CNRS, UMR 8576 – UGSF - Unité de Glycobiologie Structurale et Fonctionnelle, F-59000 Lille, France.

Tel. + 33 3 20 43 44 30

Fax. +33 3 20 43 65 55

Keywords: SLC10A7, Glycosylation, Congenital Disorders of Glycosylation, Ca2+ homeostasis, Golgi

Abstract

SLC10A7, encoded by the so-called *SLC10A7* gene, is the seventh member of a human sodium/bile acid cotransporter family, known as the SLC10 family. Despite similarities with the other members of the SLC10 family, SLC10A7 does not exhibit any transport activity for the typical SLC10 substrates and is then considered yet as an orphan carrier. Recently, *SLC10A7* mutations have been identified as responsible for a new Congenital Disorder of Glycosylation (CDG). CDG are a family of rare and inherited metabolic disorders where glycosylation abnormalities lead to multisystemic defects. SLC10A7-CDG patients presented skeletal dysplasia with multiple large joints dislocations, short stature and *amelogenesis imperfecta* likely mediated by glycosaminoglycan (GAG) defects. Although it has been demonstrated that the transporter and substrate specificities of SLC10A7, if any, differ from those of the main members of the protein family, SLC10A7 seems to play a role in Ca^{2+} regulation and is involved in proper glycosaminoglycan biosynthesis, especially heparan-sulfate, and N-glycosylation. This paper will review our current knowledge on the known and predicted structural and functional properties of this fascinating protein, and its link with the glycosylation process.

Declarations

Funding

This work was supported by grants from the Agence Nationale de la Recherche through the SKELGAG project and EUROGLYCAN-omics under the frame of E-RARE-3, the ERA-Net for Research on Rare Diseases and within the scope of the International Associated Laboratory "Laboratory for the Research on Congenital Disorders of Glycosylation – from cellular mechanisms to cure – GLYCOLAB4CDG".

Conflict of interest

The authors declare no conflict of interest.

Availability of data and material

Not applicable

Code availability

Not applicable

Author contributions

ZD and JD wrote the manuscript with support from DL, VCD and FF. Figures have been made by AL and DL. All authors discussed and revised the manuscript.

Ethics approval

Not applicable

Consent for publication

Not applicable

Introduction

Glycosylation refers to the post-translational modifications of cellular components such as lipids and/or proteins by attaching or building up glycan moieties. This highly conserved process occurs mostly in the compartments of the secretory pathway of mammalian cells (endoplasmic *reticulum* (ER) and Golgi apparatus). Glycosylation confers specific physicochemical properties needed for the cellular functions and localizations of proteins or lipids. At the protein level, the N-glycosylation starts in the ER, while other glycosylation subtypes such as O-glycosylation and/or glycosaminoglycan biosynthesis occur in the Golgi. Golgi then appears as a major cellular organelle for glycan maturation and elongation responsible for the great diversity of glycan structures found in humans. The crucial importance of glycosylation in human beings is underlined by the existence of rare and inherited diseases, so called Congenital Disorders of Glycosylation (CDG), where more than 130 different subtypes have been discovered so far and are still expanding (Ng and Freeze 2018). CDG patients present with multi systemic and metabolic disorders. As described in literature, clinical phenotypes of CDG patients are broad and can significantly differ according to the CDG subtypes, varying from skeletal manifestations to intellectual disability and seizures. In this family of diseases where genetic mutations can directly affect key players in glycosylation, such as glycosyltransferases or enzymes involved in sugar biosynthesis, a new subtype of genes has been identified in CDG over the last decade, encoding for proteins involved in Golgi homeostasis and particularly ion homeostasis. It is unambiguously the case with TMEM165-CDG (Foulquier et al. 2012). TMEM165 is indeed involved in the Golgi homeostasis regulation of Mn^{2+}, an ion absolutely required for specific Golgi glycosylation reactions (Foulquier and Legrand 2020). Interestingly, patients exhibiting mutations which lead to an impairment of ion homeostasis present with a strong bone defect phenotype. For example, TMEM165-CDG patients present with dwarfism, scoliosis, osteoporosis, and skeletal dysplasia associated with intellectual defect. In 2018, a new CDG has been discovered in patients with strong bone defects combining skeletal dysplasia with multiple large joint dislocations and an *amelogenesis imperfecta,* a defect in enamel deposition leading to abnormal enamel structure and/or quantity (Dubail et al. 2018). *SLC10A7* mutations have been identified and characterized as responsible for this CDG subtype. *SLC10A7* encodes for the SLC10A7 protein, an orphan member of the SLC10 family (Solute Carrier Family 10) that is composed of seven members. Initially identified as the Na^+/bile acid symporter family, this family contains only two members that actually function as Na^+ and bile acid cotransporters: SLC10A1 and SLC10A2 (Döring et al. 2012). The biological functions of the other members, SLC10A3, 4, 5 and 6, are still unclear. With regard to SLC10A7, the last discovered member of the SLC10 family, their cellular and biological functions are rather unknown. This review summarizes our current knowledge on SLC10A7 and its link with CDG and glycosylation.

1. SLC10A7, an orphan member of the SLC10 family

The human sodium/bile acid cotransporter family, or SLC10 family, encompasses four main protein members with reasonably-well defined cellular functions and substrates: SLC10A1, SLC10A2, SLC10A4 and SLC10A6, as well as SLC10A3, SCL10A5 and SLC10A7, three orphan members of the family. This section will briefly report our current knowledge on all these proteins, except for SCL10A7 which will be extensively described in the following parts of the manuscript.

SLC10A1 and SLC10A2, involved in the recycling of bile acids between the liver and the ileum, are by far the best characterized transporters of the family (Döring et al. 2012). Whereas SCL10A2, also called ASBT (apical sodium-dependent bile acid transporter), is found at the surface of enterocytes for the absorption of bile acids from the intestinal lumen, SLC10A1, or NTCP (Na^+-taurocholate co-transporting polypeptide), is expressed by hepatocytes for their re-absorption from portal circulation (Hagenbuch and Meier 1994, 1996; Wong et al. 1995). Both proteins act as Na^+-dependent co-transporters of bile acids like taurocholate, cholate or glycocholate, but a transport activity for sulfated steroid hormones like estrone 3-sulfate was also demonstrated for SLC10A1 (Ho et al. 2004; Craddock et al. 1998). Interestingly, mutations of *SLC10A2* have been found in Crohn's disease patients, but the link between ASBT function and Crohn's disease is still unclear (Xiao and Pan 2017). Till now, neither the structure of SLC10A1 nor that of SLC10A2 has been solved but the discovery, crystallization and characterization of two homologs of SLC10A2 in *Neisseria meningitidis* ($ASBT_{NM}$) and *Yersinia frederiksenii* ($ASBT_{Yf}$) allowed a big step forward for predicting the structure and the mechanism of Na^+/substrate cotransport of the main SLC10 proteins (Hu et al. 2011; Zhou et al. 2014).

Crystal structures of both $ASBT_{NM}$ and $ASBT_{Yf}$ revealed that the proteins possess 10 transmembrane domains (TMD), organized in two inverted repeats of five transmembrane helices forming the core and panel domains. Like their human homologs, the bacterial proteins exhibit transport activity for bile acids in a Na^+-dependent manner. Two Na^+-binding sites are present in the core domain, whose amino acid ligands are conserved in SCL10A1 and SLC10A2, and taurocholate binding in $ASBT_{NM}$ is supposed to occur in a hydrophobic cavity between the panel and core domains. Na^+ binding could induce a conformation change between the core and panel domains, thus permitting the transport of taurocholate (Hu et al. 2011; Wang et al. 2021).

Although *SLC10A3* was the first gene of the SLC10 family to be identified and expressed in a wide range of tissues (Alcalay and Toniolo 1988), it encodes for a protein whose function is still completely

unknown. The gene retrospectively found its place in the SLC10 family because of its sequence identity of about 20% with the other members of the family.

SLC10A4 is expressed in a wide range of human tissues, especially in brain, placenta and liver, and is localized both at the plasma membrane and in the intracellular compartments (Splinter et al. 2006). Unlike SLC10A1 and 2, SLC10A4 does not allow cellular taurocholate uptake except after protein cleavage by proteases, including thrombin (Abe et al. 2013). Although the cellular function of SLC10A4 is not yet fully understood, there is much evidence to qualify this protein as a transporter. Indeed, more recent studies showed that SLC10A4 is localized in synaptic vesicles (Larhammar et al, 2015). SLC10A4 expression level is correlated with dopamine uptake even if no evidence for direct transport of dopamine has been demonstrated. SLC10A4 overexpression can lead to an acidification of the synaptic vesicles, indicating a potential ionic transport activity.

SLC10A5 is a protein predominantly expressed in both liver and kidney. Its localization in the Golgi of HEK293 and U2SO cells has been demonstrated (Bijsmans et al. 2012), but its function and substrate specificity are still unknown. Indeed, it was found that SLC10A5 exhibits no transport activity for the known SLC10A1 and SLC10A2 substrates (Fernandes et al. 2007).

SLC10A6 is mainly expressed in testis, but also at relatively high levels in female tissues (breast, vagina, cervix, placenta), liver and pancreas. Functional studies revealed no transport activity for taurocholate or any other bile acid except sulfo-conjugated ones like taurolithocholic acid-3-sulfate, but SLC10A6-mediated transport in a strictly Na^+-dependent manner of sulfated steroid hormones was demonstrated (Grosser et al. 2018). Interestingly, it was shown that SLC10A6 functions may contribute to hepatic inflammation in mouse liver and macrophages (Kosters et al. 2016) and may be involved in cancer proliferation in a hormone-dependent manner (Karakus et al. 2018). Indeed, the SOAT (SLC10A6) protein, encoded by *SLC10A6* is expressed in breast adenocarcinoma, and in mammalian ductal epithelium cells. Hence, since SLC10A6 is likely involved in hormone transport in these cells, it could then be a key target in therapies against all stages of hormone-dependent breast cancer (Karakus et al. 2018).

A last member of the SLC10 family, SLC10A7, whose gene defects are responsible for CDG (SLC10A7-CDG), in contrast to any other member of the family, has been identified a few years ago. Although both SLC10A7 genetics and pathophysiology of SLC10A7-CDG have been reasonably well described, as reported in the next chapter, our current knowledge on the structure and functions of SLC10A7 explaining its role in the regulation of glycosylation processes is still sparse. This knowledge and related clues will be then reported in chapter 3.

2. SLC10A7, genetics and physiopathology: the SLC10A7-CDG

a) Gene structure

In 2005, Zou et al. performed a large-scale sequencing analysis on a human fetal brain cDNA library. Among other things, they discovered a gene of 2.7-kb, then called C4orf13. This gene contains an open reading frame encompassing nucleotides 218–1237, an in-frame codon stop between nucleotides 155 and 157, and a potential polyadenylation signal in sequence 2305-2310 (Zou et al. 2005). The whole sequence is accessible under the GenBank accession number AY346324. Two years later, Godoy et al. (2007) tried to identify novel proteins containing the SBF (Sodium Bile transporter Family - Pfam PF017) domain, which is a major amino acid sequence signature of the SLC10 family. They used NTCP and ASBT amino acids sequences as queries for GenBank Blast analysis, from which two uncharacterized sequences from mouse liver and rat colon were identified and used for RT-PCR and cDNA cloning. The authors thus obtained 1023 bp sequences exhibiting 14% identity to ASBT and NTCP. The exact same approach was then used to identify 1023 and 1032 bp transcripts from human heart and frog small intestine, respectively. The rat, mouse and human deduced protein sequences share an overall sequence identity of 94%, and the frog sequence exhibits more than 85% identity with the mammalian sequences?. Since all those protein sequences contain the typical SBF domain, the human protein was classified as the seventh member of SLC10 family: SLC10A7 (Godoy et al. 2007). The human *SLC10A7* gene is localized on 4q31 chromosome, and comprises 12 coding exons covering 222 kb, as formerly reported by Zou et al. (2005) (Fig. 1A).

Expression pattern of human *SLC10A7* has been established by RT-PCR analysis. Zou et al. (2005) found higher expression of *SLC10A7* in liver and lungs, a moderate expression in kidney, spleen and thymus, and low expression levels in heart prostate and testis, whereas Godoy et al. (2007) reported a wide *SLC10A7* expression in human tissues, with the highest expression in liver and testis. The expression pattern is similar in mice and rat, but in frog, *SLC10A7* expression was only observed in small intestine, spleen, and skeletal muscle (Godoy et al. 2007). Moreover, the expression pattern has been studied by *in situ* hybridization in mouse embryos and tissue extracts (Dubail et al. 2018). The results showed a ubiquitous expression with, except in cartilage giving birth to long bones and growth plates, where higher expression of SLC10A7 has been observed.

b) SLC10A7-CDG patient mutations

In 2018, pathogenic variants in *SLC10A7* gene were identified for the first time in humans. Those mutations were responsible for a skeletal dysplasia with *amelogenesis imperfecta*, also described now as short stature, *amelogenesis imperfecta* and skeletal dysplasia with scoliosis (SSASKS, OMIM#618363). Up to now, nine patients with autosomal recessive mutations in *SLC10A7* have been described (Ashikov et al. 2018; Dubail et al. 2018; Laugel-Haushalter et al. 2019). Among the eight pathogenic variants identified in *SLC10A7*, six were present at the homozygous state and two were compound heterozygous mutations (Table 1). More specifically, three were splice site mutations, located either in the acceptor sites of exon 9 (c.722-16 A>G), exon 10 (c.774-1 G>A), or in the donor site of exon 9 (c.773+1 G>A), four were missense mutations located in exon 3 (c.221 T>C [p.Leu74Pro]), exon 4 (c.335 G>A [p.Gly112Asp] and c.388 G>A [p.Gly130Arg]) and exon 11 (c.908 C>T [p.Pro303Leu]) and one was a nonsense mutation in exon 7 (c.514 C>T [p.Gln172*]) leading to a premature stop codon. All the identified mutations were predicted to be damaging either by PolyPhen and Sift algorithms or by transmembrane prediction software (Fig. 1A & Table1). Functional analyses indeed confirmed the deleterious impact of the mutations on cDNA and/or protein expression. These findings allowed to conclude that SSASKS was due to loss-of-function mutations in *SLC10A*7. In addition, Ashikov et al. (2018) described two other patients with similar clinical features and a complete loss of *SLC10A7* mRNA arguing for potential mutations in a regulatory element of *SLC10A7*.

c) Clinical phenotype

All patients with mutations in *SLC10A7* presented very similar clinical phenotypes, mainly characterized by pre- and postnatal short stature (<-3 SD), large joint dislocations and/or joint hyperlaxity, abnormal vertebrae with hyperlordosis or (kypho)scoliosis, hypoplastic/hypomineralised *amelogenesis imperfecta* (defective enamel formation), facial features and Pierre-Robin sequence. Apart from the two patients described by Ashikov et al. (2018), all other *SLC10A7*-deficient patients presented with advanced carpal (and tarsal) ossification in early age. Moreover, for several patients, monkey wrench appearance of the proximal femora was observed in the first months of life, which associated with short stature, large joint dislocation and advance carpal ossification, is typical of skeletal dysplasia from the group of chondrodysplasias with multiple joint dislocations (group 20 of the Nosology and Classification of genetic disorders (Mortier et al. 2019). It is noteworthy that no tooth abnormalities have been described so far for this group of dysplasia and, thus, *amelogenesis imperfecta* can be considered as a new clinical feature indicative of *SLC10A7* mutations. In most cases, *amelogenesis imperfecta* was associated with other tooth abnormalities (tooth agenesis, smaller teeth or dental crowding). Most frequently observed facial abnormalities comprised Pierre-Robin sequence (micrognathia, cleft palate and glossoptosis), micrognathia and flat face. For one patient, decreased bone mineral mass compatible with osteoporosis was detected. As it is the oldest patient described so

far, it cannot be excluded that other patients will develop with time low bone mineral mass. Finally, additional features observed included heart defect, moderate hearing impairment (mixed or sensorineural), mildly impaired intellectual development and obesity.

d) *Slc10a7*-deficient animal models

Further strengthening the implication of SLC10A7 in the physiopathology of skeletal dysplasia, two *Slc10a7*-deficient animal models were generated, both developing severe skeletal dysplasia. In the first model, *Slc10a7* was inactivated in mouse (Dubail et al. 2018). The resulting mice presented a short stature detectable at birth, larger ossified tissue in tarsal suggesting advanced ossification and craniofacial abnormalities. The growth retardation was associated with a strong disorganization of the growth plate of long bones (tissue responsible for bone growth) and a reduction of bone mass density. Furthermore, *Slc10a7*-deficient mice exhibited defects in tooth enamel consistent with *amelogenesis imperfecta*. All things considered, the *Slc10a7*-deficient mouse phenotype largely recapitulated the ones observed in *SLC10A7*-deficient human patients. In the second model, Slc10a7 was inactivated in zebrafish using morpholinos (Ashikov et al. 2018). As for mouse models, Slc10a7 morphant zebrafish presented with abnormal development of several cartilage elements and a strong reduction in bone mineralization, once again in accordance with defects described in *SLC10A7*-deficient patients.

3. Current knowledge and clues on the structure and functions of SLC10A7

a) Transcript variants and isoforms

Several transcript variants of *SLC10A7* gene have been described in literature so far, in mice but also in humans. Four variants were formerly reported by Godoy et al. (2007) in human tissues.

In a more recent study, a set of five transcript variants was reported, with a numbering from v1 to v5 (Karakus et al. 2020).. The two most expressed variants are v2 and v4, variant v2 corresponding to the full-length transcript of *SLC10A7* gene. Those transcript variants are summarized in Figure 1B. Variant v4 differs from variant v2 because of an alternative splicing event that leads to the additional transcription of exon 11'. Because of this alternative splicing, exon 12 is non-coding, leading the proteins encoded by variant v2 and v4 to have different C-termini: the protein coded by v2 has a C-t end encoded by exon 12 while the protein coded by v4 has a C-t end from exon 11'. Karakus et al. (2020) showed that only v2 and v4 are expressed, and that their expression occurs in most human tissues, although with slightly different specificities. Variant v2 is indeed found predominant in the urinary bladder, while v4 is more expressed in the salivary gland.

Other variants, v1, 3 and 5, could not be detected in this study. Variant v1 is a non-sense mRNA decay variant, its transcription being off frame due to a premature stop codon and a skip of exons 8 and 9. Variant v3 is only made of exons 1 to 4, with an additional alternative exon 4'. The fifth variant (v5) results from the skip of exon 5. The proteins encoded by those variants are accessible on NCBI, under the accession numbers NP_001025487 (v1), NP_001025169 (v2), NP_115504 (v3), NP_001287771 (v4) and NP_001304745 (v5). They encode for the SLC10A7 protein isoforms a, b, c, d and e, respectively (Fig. 1B). Since variant v1 comes from a non-sense mRNA decay, its encoded protein (isoform a) has been suppressed from the database (Karakus et al. 2020).

At last, two other variants (v6 and v7) can be found in GenBank. Their expression and coding isoform have not been studied. It is important to note that discrepancies may be found throughout the literature as regards *SLC10A7* gene and variant expressions in human tissues and organs. The G-TEX portal for *SLC10A7* (https://gtexportal.org/home/gene/SLC10A7) shows a lower expression of *SLC10A7* in brain, blood and skeletal muscle, and a higher expression in transformed lymphocytes, nerves, and thyroid. Relative expression in bones is not described.

b) Protein primary structure and predicted membrane topology

The full-length SLC10A7 protein (isoform b from transcript variant v2) is composed of 340 amino acids whose sequence is illustrated in Figure 2A. Although a molecular mass of 37.4 kDa may be calculated for the protein, immunoprecipitation of FLAG-tagged SLC10A7 from HEK293 cells led to the detection of two specific bands in western-blot, a major band of 27 kDa and a fainter band of 54 kDa. Since no predictive N-glycosylation sites were found in SLC10A7, it was hypothesized that the second band could represent protein dimers (Godoy et al. 2007). In support to this, it has indeed been shown that dimerization, homo and hetero dimerization, is a common characteristic within the SLC10 family (Noppes et al. 2019). The Sodium Bile Family (SBF) domain found in SLC10A7 (residues 44-205) shares a 12-16% identity with the other SLC10 family members (Godoy et al. 2007). Bioinformatics studies formerly predicted a membrane topology model of either 10 or 9 TMDs. In the 10 TMD model, N and C-termini have been predicted as intracellular, while in the 9 TMD model, the N-t end was predicted to be intracellular and the C-t end extracellular. Actually, owing to strategical insertion of HA and FLAG tags in the SLC10A7 protein expressed in HEK293T cells, followed by immunofluorescence staining with different permeabilization protocols, the 10 TMD model has been validated (Godoy et al. 2007) (Fig. 2). According to these findings, and by referring to the structural homologies of SLC10A7 with bacterial homologs $ASBT_{NM}$ and $ASBT_{Yf}$, the structure of the protein may be predicted, and is presented in section 3c (Fig. 2).

c) Predicted 3D structure

Till now, as mentioned in section 1, none of the proteins of the SLC10 family have seen their structure experimentally characterized. However, the crystal structure in detergent conditions of a bacterial SLC10 homolog from *N. meningitidis* ($ASBT_{NM}$) (Hu et al. 2011), followed by the structure in a lipid environment of its homolog from *Y. frederiksenii* ($ASBT_{Yf}$) (Zhou et al. 2014; Wang et al. 2021), has been solved. This was particularly useful for predicting the structures of proteins with similar Na^+-bile acid cotransport functions, most especially SLC10A1 and SLC10A2, as reported earlier (Döring et al. 2012; Claro da Silva et al. 2013). Despite the fact that SLC10A7 markedly differs from the other SLC10 family members, owing to its low sequence identity, higher gene complexity, main location within the secretory pathway, and the evidence that it is not a transporter of bile acids. strong structure homologies may also be found between SCL10A7 and the bacterial ASBT homologs, most particularly $ASBT_{Yf}$. (Fig. 2). Like $ASBT_{Yf}$ and $ASBT_{NM}$, SCL10A7 is predicted to have 10 domains with both N- and C-t ends towards the cytosolic side (Fig. 2A). Interestingly, the predicted SLC10A7 scaffold is very similar to that of bacterial ASBT, with a core domain dedicated to the binding of ions, and a panel domain delimiting a large cavity likely involved for the binding and transport of an organic compound (Fig. 2B & C, grayed area A). This strongly suggests that SLC10A7 may act, in a similar way to bacterial ASBT, human SLC10A1 and SLC10A2, as a transporter of organic molecules, which still need to be characterized. Furthermore, the overall folding of the core domain seems to be homologous to the Na^+-bile acid cotransporters, most particularly with the presence of a central cavity containing the two Na^+-binding sites, mentioned in section 1, mainly formed at the interface between the non-helical segments of TM4 and TM9 (residues 113-121 and 277-281) (Fig. 2A and Fig. 2B & C, grayed area B). However, it may be observed that most residues involved in both Na^+-binding sites 1 and 2 of $ASBT_{Yf}$ (Zhou et al. 2014; Wang et al. 2021) whose homologous positions on SLC10A7 are indicated in Figure 2A by the yellow- and green-circled amino acids, are poorly conserved. More particularly, two amino acids of TM9 critical for binding Na^+ in $ASBT_{Yf}$, E_{254} and Q_{258}, highly conserved in SLC10A1 and SLC10A2, are found as C_{274} and K_{278} in SLC10A7. Those two amino acids are extremely conserved in SLC10A7 orthologs (personal data). This strongly suggests that the transport function of SLC10A7, if any, may not depend on Na^+ binding. Interestingly, it may be observed that all single point mutations found in SLC10A7-CDG patients and reported in section 2, except for P_{301}, are located within the core domain, at the vicinity of the amino acids potentially involved in ion binding.

d) Protein localization

Given the lack of SCL10A7-specific antibodies suitable for immunochemistry, the subcellular localization of the protein is not completely solved yet. The use of different SLC10A7 tagged forms and cellular models, led to different observations. First, Godoy at al. (2007) found most of SLC10A7 localized at the plasma membrane in HEK293T cells, with a non negligeable part in the ER. While such expression at the plasma membrane was further supported using the same cell line (Dubail et al. 2018), and also for Rch1p, the SLC10A7 yeast ortholog (Jiang et al. 2012), the localization of SLC10A7 was reported along the compartments of the secretory pathway in several studies. In particular, a specific Golgi distribution of SCL10A7 in both HeLa cells and human fibroblasts was demonstrated by Ashikov et al. (2018). This however does not seem to be restricted to the Golgi as an ER localization of SLC10A7, colocalizing with other ER-specific proteins like STIM1, was observed in HAP1 cells (Karakus et al. 2020).

Although all these data do not allow to precisely define the subcellular localization of SLC10A7, which probably differs according to the type and physiological status of cells, they reasonably support its presence in the different compartments of the secretory pathway, and more especially in the Golgi where the maturation of glycans and glycosaminoglycans occurs.

e) Link with Ca^{2+} homeostasis

CaRch1 and ScRch1, two orthologs of SLC10A7 in *Candida albicans* and *Saccharomyces cerevisiae*, respectively, helped to highlight the function of SLC10A7 in cellular Ca^{2+} homeostasis (Jiang et al. 2012; Zhao et al. 2016). This link was further confirmed through experiments in human cells (Karakus et al. 2020).

Indeed, it has been shown that in Δ-CaRch1 *C. albicans* cells, the Ca^{2+} entry in cells is increased, together with the cytosolic Ca^{2+} levels, leading to a strong activation of the calcineurin pathway. This pathway is activated in presence of high Ca^{2+} concentrations and is used by yeasts to decrease the Ca^{2+} quantity in the cytoplasm: Ca^{2+} can activate the calcineurin phosphatase, that will itself dephosphorylate and activate Crz1, a transcription factor that will increase the transcription of genes involved in Ca^{2+} storage in organelles (like *Pmr1*) or Ca^{2+} efflux at the plasma membrane (Jiang et al. 2012). In a study by Zhao et al (Zhao et al. 2016), the authors demonstrated that, shortly after an important extracellular Ca^{2+} pressure, Rch1 is overexpressed *via* the calcineurin pathway and found at the plasma membrane, especially at the bud in budding yeast and in a few intracellular puncti. It is assumed that such Rch1 overexpression aims at negatively regulating Ca^{2+} homeostasis at the plasma membrane to fine tune intracellular Ca^{2+} homeostasis and provide negative feedback on the calcineurin pathway. Although the transport activity of Rch1 and its exact cellular functions have not

been characterized yet, these data clearly indicate that the yeast SCL10A7 homolog acts, directly or indirectly, as a negative regulator of cytosolic Ca^{2+} (Zhao et al. 2016).

In human cells, the cellular Ca^{2+} entry mostly occurs *via* the Store Operated Channels (SOC). These channels that are expressed at the plasma membrane transport extracellular Ca^{2+} into the cytoplasm. ORAI1 is the main SOC in human cells. As illustrated in Figure 3 (adapted from Lu and Fivaz 2016), depletion of Ca^{2+} from the ER store leads to the oligomerization of STIM1 proteins, then acting as a direct reticular sensor of Ca^{2+} concentration. Once oligomerized STIM1 then triggers the activation of the plasma membrane channels ORAI1, by interacting with ORAI1 at ER/plasma membrane contact puncti. This leads to a cellular Ca^{2+} entry in the cytoplasm *via* these ORAI1 channels. The cytosolic Ca^{2+} is then transported and relocalized from the cytoplasm into the ER *via* the SERCA pumps, thus allowing repletion of ER Ca^{2+} stores (Fig. 3). Very interestingly, Karakus et al. (Karakus et al. 2020) showed that in SLC10A7 KO HAP1 cells, Ca^{2+} entry *via* the SOC channels is increased, as compared to wild-type HAP1 cells, whereas the overexpression of SLC10A7 in those cells inhibits the SOC-dependent Ca^{2+} entry. These results then strongly suggest that SLC10A7 expression is negatively correlated with the SOC-dependent Ca^{2+} entry in cells. In addition, the authors showed that the overexpression of mutated SLC10A7 patient forms does not rescue the Ca^{2+} entry increase in SLC10A7 KO HAP1 cells, thus indicating that the mutations affect the functionality of SLC10A7. At last, they found that SLC10A7 co-localizes with STIM1 and SERCA in the ER, and thus hypothesized that SLC10A7 may be a regulator of one or more of those proteins involved in Ca^{2+} homeostasis in human cells (Karakus et al. 2020) (illustrated in Fig 3).

Remarkably, most patients having genetic mutations affecting STIM1 or ORAI1 functionality present with an *amelogenesis imperfecta* and hypocalcification of enamel, two specific clinical phenotypes associated to SLC10A7-CDG patients (Lacruz and Feske 2015). This strongly supports the hypothesis of a link between SLC10A7 and the STIM1/ORAI1 pathway in regulating cellular Ca^{2+} homeostasis and this observed specific phenotype.

Since Ca^{2+} has pleiotropic cellular roles, it may be expected that any deficiency of SLC10A7 might negatively impact many cellular mechanisms, including of course the glycosylation processes, as reported thereafter, but also any other intracellular signaling and trafficking process.

f) Impact of SLC10A7 deficiency on glycosylation

The importance of SLC10A7 for glycosylation has emerged with the discovery by Ashikov et al. (2018) of *SLC10A7* mutations in CDG patients exhibiting glycosylation defects but no mutations in already-identified CDG-linked genes. This allowed the identification of *SLC10A7* gene deficiencies as a

cause of a new CDG and the observation of a characteristic glycosylation signature for this specific CDG. In particular, some abnormalities in N-glycan biosynthesis, especially occurring in the Golgi part of the N-glycan maturation process, were depicted by glycomic analysis of patient plasma glycoproteins. N-glycosylation is initiated in the ER by the en bloc transfer of the oligosaccharide precursor onto proteins. This precursor is composed of two types of carbohydrates: N-acetylglucosamine and mannoses. Then, the proteins are sent to the Golgi apparatus where their N-glycans are matured, to include N-acetylglucosamine, mannose, galactose and terminal sialic acid residues. However, in SLC10A7-CDG patients, high-mannose N-glycans, only composed of N-acetylglucosamine and mannose residues, are overrepresented, and the sialylation degree of complex (mature) N-glycans is decreased. Those N-glycans abnormalities are rather difficult to understand but indicate that SLC10A7 deficiency disturbs many steps of the N-glycan maturation through the different cisterna of the Golgi apparatus (Ashikov et al. 2018). In addition to the observed N-glycan defects, an impact on the biosynthesis of glycosaminoglycans have been reported in both SLC10A7 patients' fibroblasts and SLC10A7 KO mice (Dubail et al. 2018). Although the total GAG contents of patient fibroblasts and cartilage extracts of SLC10A7 KO mice were unchanged as compared to controls, the amount of heparan-sulfate (HS) was surprisingly significantly decreased, with about 2- and 2.5-fold less HS found in SLC10A7-deficient fibroblasts and SLC10A7 KO mice cartilage extracts, respectively. Since those HS chains were sulfated and had a length similar to HS chains of control cells, it was concluded that the defect in HS chains was more quantitative than qualitative. The amounts of chondroitin-sulfate (CS) chains were also assessed by immunostaining in growth plates of control and SLC10A7 KO mice. Unlike HS, no decreased amounts of CS could be observed, but a higher density of CS at close proximity of chondrocytes in KO mice than in control mice was found (Dubail et al. 2018).

As depicted in Figure 4, which illustrates the impacts of SLC10A7 deficiency on both N-glycosylation and GAG biosynthesis pathways, GAG biosynthesis starts in the Golgi by the synthesis of a linker, common to all GAG subtypes. The difference between CS and HS deals with the transfer to the linker of a GalNAc by the CSGalNACT1/2 or a GlcNAc by the EXTL1-3, respectively (Chen et al. 2018). Since SLC10A7 deficiency decreases the amounts for HS, not CS, it may be assumed that the GAG linker biosynthesis is not affected by the deficiency. In contrast, although this cannot still be explained, the glycosyltransferases involved in HS biosynthesis, but not CS, seem to be impacted by SLC10A7 deficiency. Interestingly, other genetic diseases affecting the biosynthesis of GAGs, such as EXTL1-3-CDG, caused by a defect of the N-acetylglucosaminyltransferase I involved in the initiation of elongation of HS chains, also exhibit a clinical phenotype including a bone mineralization defect or skeletal dysplasia (Volpi et al. 2017).

Of course, it cannot be excluded that the Ca^{2+} homeostasis impairment, caused by SLC10A7 deficiency, leads to the abnormal glycosylation phenotype. Indeed, the observed intracellular Ca^{2+} increase could affect the transcription level, vesicular trafficking speed and activity of any protein involved in Golgi glycosylation process. In particular, it is worthy to remind that the availability of both Ca^{2+} and Mn^{2+} in the organelles is an important factor for Golgi glycosylation. Actually, the first Golgi mannosidases involved in the trimming of high mannose N-glycans are Ca^{2+} dependent while most of the Golgi glycosyltransferases require Mn^{2+} as cofactor. Hence, it is likely that any imbalance of ion homeostasis would lead to specific Golgi glycosylation defects.

To summarize, SLC10A7 deficiency impairs N-glycan maturation and sialylation, HS expression and CS localization thus affecting a large diversity of glycosylation processes in the Golgi apparatus, from the ERGIC to the trans-Golgi network (Fig. 3).

Conclusion

Although the exact intracellular localization of SLC10A7 still needs to be outlined, the strong impact of its deficiency on glycosylation, all along the secretory pathway, together with the link with Ca^{2+} homeostasis, highlights this putative transporter as a key player in ER/ Golgi ion homeostasis as well as glycosylation. Unravelling the role of SLC10A7 in Golgi ion homeostasis could then lead to the discovery of simple new therapeutic pathways for SLC10A7-CDG patients, as it was the case for TMEM165-CDG (Houdou et al. 2019). Ion transport and regulation in the Golgi apparatus are still poorly understood, and their crucial roles in Glycosylation processes has clearly been underestimated. Future research are needed to disentangle the function of SLC10A7 in Golgi ion homeostasis regulation and Golgi glycosylation process.

Legends to Table and Figures

Table 1 : Mutations in SLC10A7-CDG patients (inspired from Karakus et al. 2020)

Figure 1: SLC10A7 genomic organization and transcript variant representation

A Schematic representation of SLC10A7 genomic coding sequence. It is divided into 12 exons (white-numbered blue boxes). The length of each exon is proportional to their base content. The introns are not scaled. The numbering under each exon is based on coding nucleotides (Zou et al. 2005). cDNA Patients mutations are spotted with red arrows and noted in red. **B** SLC10A7 most common variants,

v2 and v4. Exon 11' is only present in v4 whose exon 12 represented with a dotted line is non coding. Each variant can be found by an Ensembl transcript number annotated under the sequence.

Figure 2: Predicted topology and 3D structure of SLC10A7

A search on the PHYRE2 server (http://www.sbg.bio.ic.ac.uk/-~phyre2/) using the human SLC10A7 isoform b protein chain (UniProtKB/Swissprot ID Q0GE19-2) indicates a 100% probability/confidence that amino acid residues 6-332 of SLC10A7 match with the apical sodium-dependent bile acid transporter (ASBT; also known as SLC10A2) homologue from *Yersinia frederiksenii* ($ASBT_{Yf}$) whose structure in a lipid environment was solved at 1.95 Å resolution (PDB entry 4N7W, Zhou et al. 2014). This ultimate homology probability, together with a 21% sequence identity between SLC10A7 and $ASBT_{Yf}$, give reasonably accurate the topology model depicted in the scheme in panel A and the overall SLC10A7 fold shown in panels B and C. (A) Putative schematic 2D topology of the human SLC10A7 isoform b protein chain showing the 10 transmembrane domains (TM1-TM10) predicted by both TMHMM v.2.0 (http://www.cbs.dtu.dk/services/TMHMM/) and PHYRE2 servers. Both N- (N-t) and C-terminal (C-t) ends are located at the cytosolic side. The transmembrane segments belonging to the predicted functional domains of SLC10A7 described in the text and illustrated in B and C, namely the core domain (TM3-5, TM8-10) and the panel domain (TM1-2, TM6-7), are indicated. The luminal side and cytoplasmic loops are indicated as L1-L5 and C1-C4, respectively. The one-letter-code amino acids in the black- grey- and white-filled circles correspond to the identical, highly similar and non-conserved residues between SLC10A7 and $ASBT_{Yf}$, respectively, as determined by primary sequence alignments in Clustal Omega (https://www.ebi.ac.uk/Tools/msa/clustalo/) (Madeira et al. 2019). The red-circled amino acids are those found mutated in SLC10A7-CDG patients (see section 3 of the manuscript), with red arrows indicating the amino acid changes. The yellow- and green-circled amino acids are located at positions corresponding to the residues identified in the Na^+-binding sites 1 and 2 of $ASBT_{Yf}$, respectively (Zhou et al. 2014; Wang et al. 2021). (B and C) Model of SLC10A7 predicted on PHYRE2 using the structure of $ASBT_{Yf}$ (PDB entry 4N7W) as a template. Rainbow-color fold representation was obtained using the UCSF ChimeraX software (Goddard et al. 2018). The numbering of TM domains and loops is the same as in panel A. The side view (B) and the top view (C) of the predicted SLC10A7 model are shown. The core and panel domains are indicated. The grayed areas roughly indicate the locations of the bile acid pocket (area A) and the two Na^+-binding sites (area B) characterized in $ASBT_{Yf}$ (Zhou et al. 2014; Wang et al. 2021).

Figure 3: Negative regulation by SLC10A7 of SOC-dependent cellular Ca^{2+} entry in response to ER Ca^{2+} depletion.

This scheme, inspired from Lu and Fivaz (2016), shows the principal molecular components (ORAI1 and STIM1) and their interactions permitting the store operated Ca^{2+} entry (SOCE). When ER Ca^{2+} stores are full (left side), STIM1 is dispersed throughout the ER. In conditions of ER Ca^{2+} depletion, STIM1 oligomerizes (red arrows), recruits and interacts with ORAI1 at ER-PM contact sites, then allowing cellular Ca^{2+} entry (blue arrows) and replenishing of stores *via* the SERCA pumps. SLC10A7, mainly expressed in the secretory pathway, ER and/or Golgi, seems to act as a negative regulator of SOC-dependent Ca^{2+} ER replenishing by possibly interacting with one or more components of this pathway (ORAI1, STIM1 and/or SERCA) (black arrows). The solute transport activity of SLC10A7, still not characterized (green arrows), may also account for the negative regulation of Ca^{2+} entry and storage. Figure was built using Servier Medical Art graphics (smart.servier.com).

Figure 4: Schematic representation of the impact of SLC10A7 on the N-glycosylation process and heparan sulfate biosynthesis

SLC10A7 deficiency impacts glycosylation processes in the different cellular compartments and Golgi cisterna represented. N-glycosylation and heparan sulfate (HS) synthesis (red frames) are affected. Regarding N-glycans maturation, high mannose structures such as Man9GlcNAc2 increase. A decrease in the sialylation degree of complex N-glycans is also found. Heparan Sulfate biosynthesis is affected in SLC10A7 deficiency. A general decrease is observed but without affecting the quality of the HS structures. The substitution of the glycans is not fully represented; only the remaining structure at the entrance of each cisterna is shown. Phosphorylation is represented by the letter « P ». The symbol nomenclature for glycan structure is depicted in the bottom left-hand corner.

References

Abe T, Kanemitu Y, Nakasone M, et al (2013) SLC10A4 is a protease-activated transporter that transports bile acids. J Biochem 154:93–101. https://doi.org/10.1093/jb/mvt031

Alcalay M, Toniolo D (1988) CpG islands of the X chromosome are gene associated. Nucleic Acids Res 16:9527–9543. https://doi.org/10.1093/nar/16.20.9527

Ashikov A, Abu Bakar N, Wen X-Y, et al (2018) Integrating glycomics and genomics uncovers SLC10A7 as essential factor for bone mineralization by regulating post-Golgi protein transport and glycosylation. Human Molecular Genetics 27:3029–3045. https://doi.org/10.1093/hmg/ddy213

Bijsmans ITGW, Bouwmeester RAM, Geyer J, et al (2012) Homo- and hetero-dimeric architecture of the human liver Na^+-dependent taurocholate co-transporting protein. Biochem J 441:1007–1015. https://doi.org/10.1042/BJ20111234

Chen Y-H, Narimatsu Y, Clausen TM, et al (2018) The GAGOme: a cell-based library of displayed glycosaminoglycans. Nat Methods 15:881–888. https://doi.org/10.1038/s41592-018-0086-z

Claro da Silva T, Polli JE, Swaan PW (2013) The solute carrier family 10 (SLC10): Beyond bile acid transport. Molecular Aspects of Medicine 34:252–269. https://doi.org/10.1016/j.mam.2012.07.004

Craddock AL, Love MW, Daniel RW, et al (1998) Expression and transport properties of the human ileal and renal sodium-dependent bile acid transporter. Am J Physiol 274:G157-169. https://doi.org/10.1152/ajpgi.1998.274.1.G157

Döring B, Lütteke T, Geyer J, Petzinger E (2012) The SLC10 carrier family: transport functions and molecular structure. Curr Top Membr 70:105–168. https://doi.org/10.1016/B978-0-12-394316-3.00004-1

Dubail J, Huber C, Chantepie S, et al (2018) SLC10A7 mutations cause a skeletal dysplasia with amelogenesis imperfecta mediated by GAG biosynthesis defects. Nat Commun 9:3087. https://doi.org/10.1038/s41467-018-05191-8

Foulquier F, Amyere M, Jaeken J, et al (2012) TMEM165 Deficiency Causes a Congenital Disorder of Glycosylation. The American Journal of Human Genetics 91:15–26. https://doi.org/10.1016/j.ajhg.2012.05.002

Foulquier F, Legrand D (2020) Biometals and glycosylation in humans: Congenital disorders of glycosylation shed lights into the crucial role of Golgi manganese homeostasis. Biochim Biophys Acta Gen Subj 1864:129674. https://doi.org/10.1016/j.bbagen.2020.129674

Goddard TD, Huang CC, Meng EC, et al (2018) UCSF ChimeraX: Meeting modern challenges in visualization and analysis. Protein Sci 27:14–25. https://doi.org/10.1002/pro.3235

Godoy JR, Fernandes C, Döring B, et al (2007) Molecular and phylogenetic characterization of a novel putative membrane transporter (SLC10A7), conserved in vertebrates and bacteria. European Journal of Cell Biology 86:445–460. https://doi.org/10.1016/j.ejcb.2007.06.001

Grosser G, Bennien J, Sánchez-Guijo A, et al (2018) Transport of steroid 3-sulfates and steroid 17-sulfates by the sodium-dependent organic anion transporter SOAT (SLC10A6). The Journal of Steroid Biochemistry and Molecular Biology 179:20–25. https://doi.org/10.1016/j.jsbmb.2017.09.013

Hagenbuch B, Meier PJ (1994) Molecular cloning, chromosomal localization, and functional characterization of a human liver Na+/bile acid cotransporter. J Clin Invest 93:1326–1331

Hagenbuch B, Meier PJ (1996) Sinusoidal (basolateral) bile salt uptake systems of hepatocytes. Semin Liver Dis 16:129–136. https://doi.org/10.1055/s-2007-1007226

Ho RH, Leake BF, Roberts RL, et al (2004) Ethnicity-dependent polymorphism in Na+-taurocholate cotransporting polypeptide (SLC10A1) reveals a domain critical for bile acid substrate recognition. J Biol Chem 279:7213–7222. https://doi.org/10.1074/jbc.M305782200

Houdou M, Lebredonchel E, Garat A, et al (2019) Involvement of thapsigargin- and cyclopiazonic acid-sensitive pumps in the rescue of TMEM165-associated glycosylation defects by Mn2. FASEB J 33:2669–2679. https://doi.org/10.1096/fj.201800387R

Hu N-J, Iwata S, Cameron AD, Drew D (2011) Crystal structure of a bacterial homologue of the bile acid sodium symporter ASBT. Nature 478:408–411. https://doi.org/10.1038/nature10450

Jiang L, Alber J, Wang J, et al (2012) The Candida albicans plasma membrane protein Rch1p, a member of the vertebrate SLC10 carrier family, is a novel regulator of cytosolic Ca2+ homoeostasis. Biochem J 444:497–502. https://doi.org/10.1042/BJ20112166

Karakus E, Wannowius M, Müller SF, et al (2020) The orphan solute carrier SLC10A7 is a novel negative regulator of intracellular calcium signaling. Scientific Reports 10:. https://doi.org/10.1038/s41598-020-64006-3

Karakus E, Zahner D, Grosser G, et al (2018) Estrone-3-Sulfate Stimulates the Proliferation of T47D Breast Cancer Cells Stably Transfected With the Sodium-Dependent Organic Anion Transporter SOAT (SLC10A6). Front Pharmacol 9:. https://doi.org/10.3389/fphar.2018.00941

Kosters A, Abebe DF, Felix JC, et al (2016) Inflammation-associated upregulation of the sulfated steroid transporter Slc10a6 in mouse liver and macrophage cell lines: Slc10a6 upregulation in hepatic inflammation. Hepatol Res 46:794–803. https://doi.org/10.1111/hepr.12609

Lacruz RS, Feske S (2015) Diseases caused by mutations in ORAI1 and STIM1. Ann N Y Acad Sci 1356:45–79. https://doi.org/10.1111/nyas.12938

Lairson LL, Henrissat B, Davies GJ, Withers SG (2008) Glycosyltransferases: Structures, Functions, and Mechanisms. Annu Rev Biochem 77:521–555. https://doi.org/10.1146/annurev.biochem.76.061005.092322

Laugel-Haushalter V, Bär S, Schaefer E, et al (2019) A New SLC10A7 Homozygous Missense Mutation Responsible for a Milder Phenotype of Skeletal Dysplasia With Amelogenesis Imperfecta. Front Genet 10:504. https://doi.org/10.3389/fgene.2019.00504

Lu B, Fivaz M (2016) Neuronal SOCE: Myth or Reality? Trends Cell Biol 26:890-893. https://doi.org/10.1016/j.tcb.2016.09.008

Madeira F, Park Y mi, Lee J, et al (2019) The EMBL-EBI search and sequence analysis tools APIs in 2019. Nucleic Acids Research 47:W636–W641. https://doi.org/10.1093/nar/gkz268

Mortier GR, Cohn DH, Cormier-Daire V, et al (2019) Nosology and classification of genetic skeletal disorders: 2019 revision. Am J Med Genet A 179:2393–2419. https://doi.org/10.1002/ajmg.a.61366

Ng BG, Freeze HH (2018) Perspectives on Glycosylation and Its Congenital Disorders. Trends in Genetics 34:466–476. https://doi.org/10.1016/j.tig.2018.03.002

Noppes S, Müller SF, Bennien J, et al (2019) Homo- and heterodimerization is a common feature of the solute carrier family SLC10 members. Biological Chemistry 400:1371–1384. https://doi.org/10.1515/hsz-2019-0148

Potelle S, Morelle W, Dulary E, et al (2016) Glycosylation abnormalities in Gdt1p/TMEM165 deficient cells result from a defect in Golgi manganese homeostasis. Human Molecular Genetics 25:1489–1500. https://doi.org/10.1093/hmg/ddw026

Splinter PL, Lazaridis KN, Dawson PA, LaRusso NF (2006) Cloning and expression of SLC10A4, a putative organic anion transport protein. World J Gastroenterol 12:6797–6805. https://doi.org/10.3748/wjg.v12.i42.6797

Volpi S, Yamazaki Y, Brauer PM, et al (2017) EXTL3 mutations cause skeletal dysplasia, immune deficiency, and developmental delay. J Exp Med 214:623–637. https://doi.org/10.1084/jem.20161525

Wang X, Lyu Y, Ji Y, et al (2021) Substrate binding in the bile acid transporter ASBT $_{Yf}$ from *Yersinia frederiksenii*. Acta Crystallogr D Struct Biol 77:117–125. https://doi.org/10.1107/S2059798320015004

Wong MH, Oelkers P, Dawson PA (1995) Identification of a mutation in the ileal sodium-dependent bile acid transporter gene that abolishes transport activity. J Biol Chem 270:27228–27234. https://doi.org/10.1074/jbc.270.45.27228

Xiao L, Pan G (2017) An important intestinal transporter that regulates the enterohepatic circulation of bile acids and cholesterol homeostasis: The apical sodium-dependent bile acid transporter (SLC10A2/ASBT). Clinics and Research in Hepatology and Gastroenterology 41:509–515. https://doi.org/10.1016/j.clinre.2017.02.001

Zhao Y, Yan H, Happeck R, et al (2016) The plasma membrane protein Rch1 is a negative regulator of cytosolic calcium homeostasis and positively regulated by the calcium/calcineurin signaling pathway in budding yeast. European Journal of Cell Biology 95:164–174. https://doi.org/10.1016/j.ejcb.2016.01.001

Zhou X, Levin EJ, Pan Y, et al (2014) Structural basis of the alternating-access mechanism in a bile acid transporter. Nature 505:569–573. https://doi.org/10.1038/nature12811

Zou X, Wang D, Qiu G, et al (2005) Molecular Cloning and Characterization of a Novel Human C4orf13 Gene, Tentatively a Member of the Sodium Bile Acid Cotransporter Family. Biochem Genet 43:165–173. https://doi.org/10.1007/s10528-005-1509-y

Table 1

Nucleotide change	Amino acid change	Location	Status	Comment
c.221T>C	Leu74Pro	Exon 3	Homozygous	Mutation affects a highly conserve amino acid in the third predicted transmembrane helix
c.335G>A	Gly112Asp	Exon 4	Compound Heterozygous with c.722-16A<G	Mutation leads to the disruption of the fourth transmembrane domain
c.388G>A	Gly130Arg	Exon 4	Homozygous	Missense mutation which affects a highly conserve amino acid
c.514C>T	Gln172*	Exon 7	Homozygous	Mutation leads to a premature codon stop
c.722-16A>G	Gly112ASP	Intron 8	Compound Heterozygous with c.335G>A	Premature codon stop. Exon 9 skipped
c.773+1G>A	?	Intron 9	Homozygous	Splice mutations in intron 9 leading to exon 9 skipping.
c.774-1G>A	?	Intron 9	Homozygous	Splice mutations in intron 9 leading to exon 10 skipping
c.908C>T	Pro303Leu	Exon 11	Homozygous	Mutation in the tenth transmembrane domain
-	-	-	-	Absence of SLC10A7 cDNA and complete loss of SLC10A7 protein

Abbreviations

CDG, Congenital Disorders of Glycosylation; GAG, glycosaminoglycans

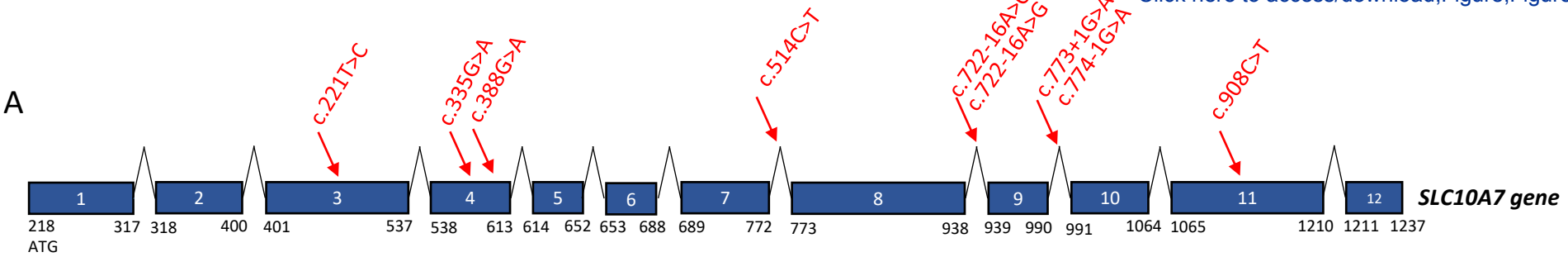

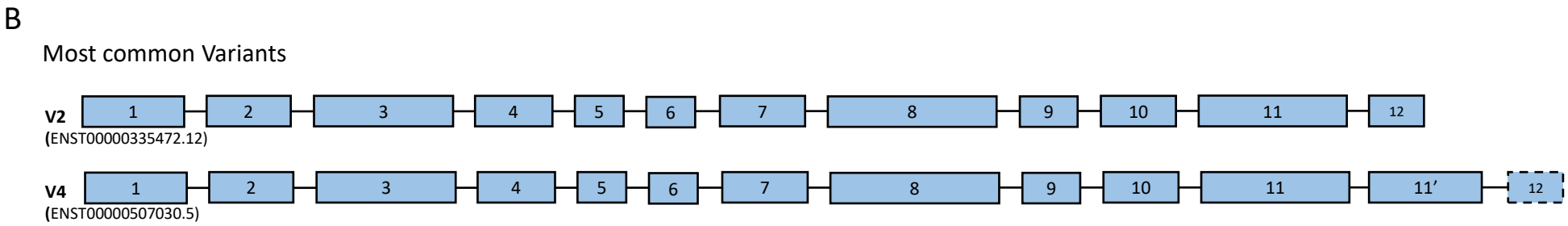

FIGURE 1

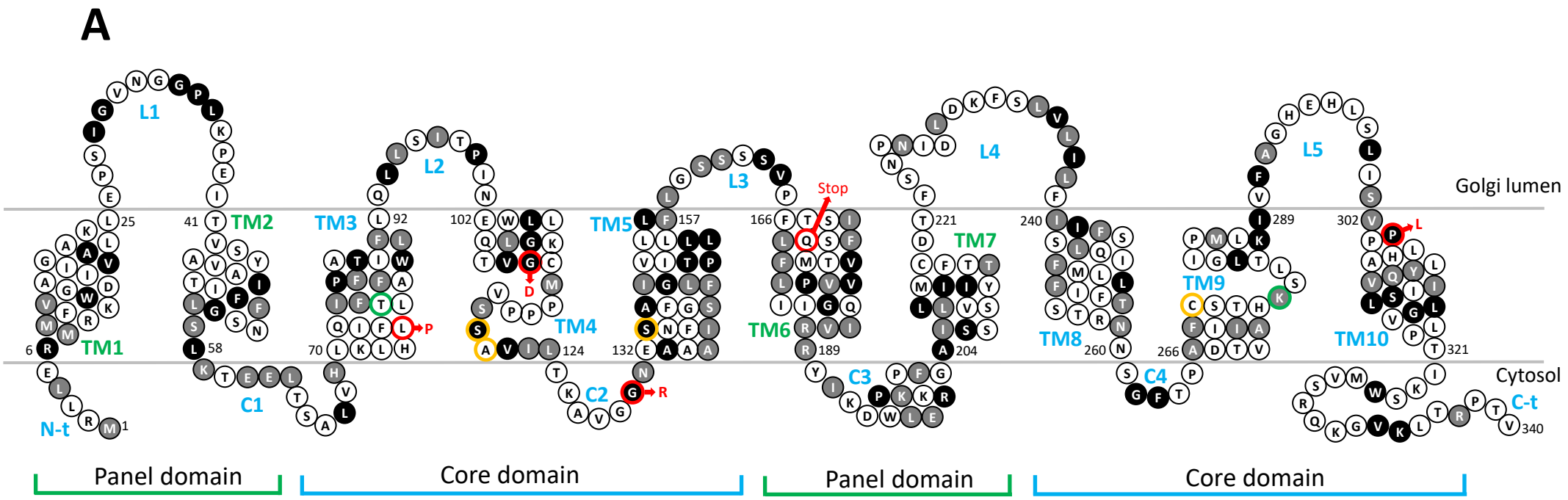
A
L1
L2
L3
L4
L5
TM1
TM2
TM3
TM4
TM5
TM6
TM7
TM8
TM9
TM10
C1
C2
C3
C4
N-t
C-t
Stop
Golgi lumen
Cytosol
Panel domain
Core domain
Panel domain
Core domain

FIGURE 2

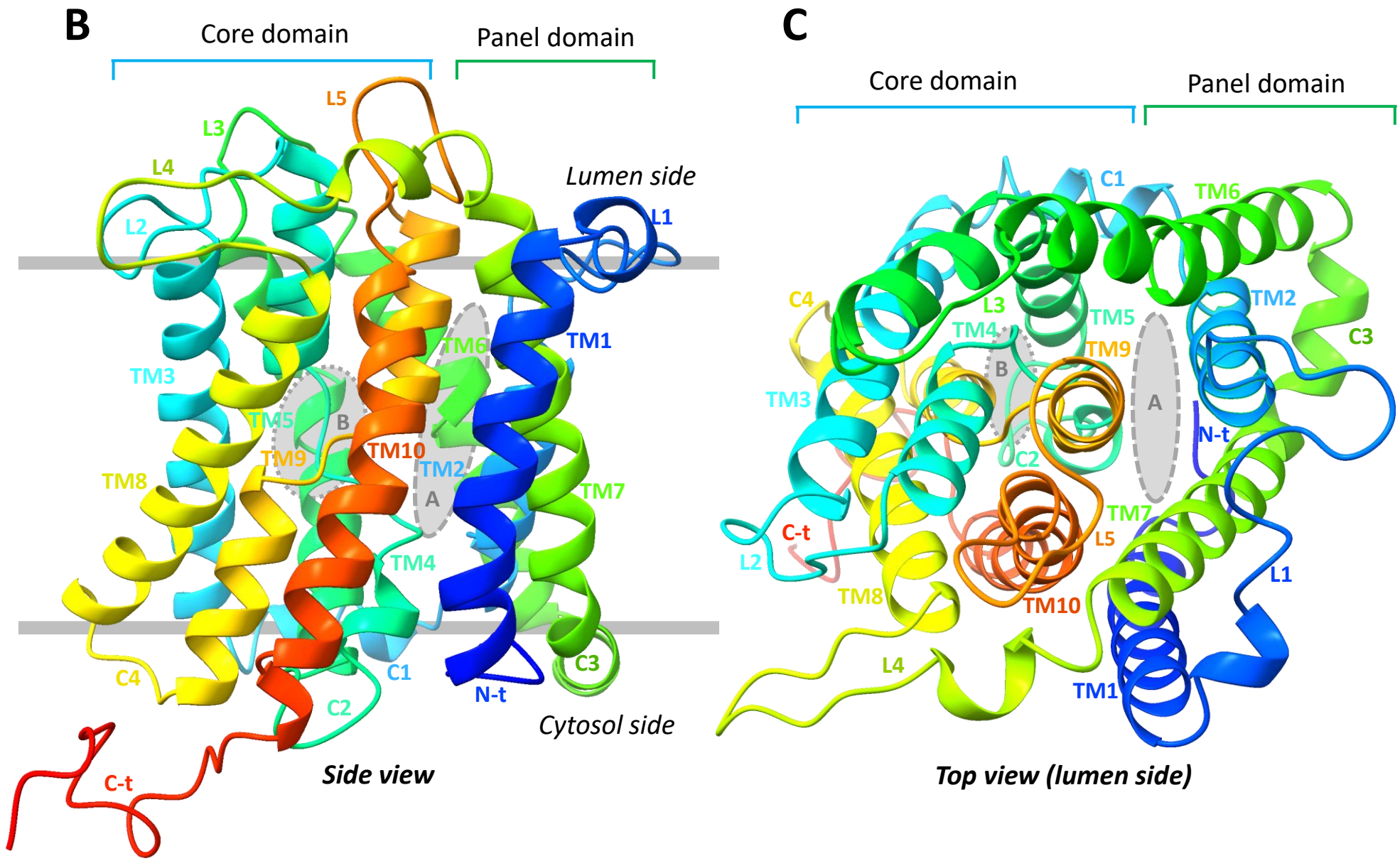
B
Core domain
Panel domain
L5
L3
L4
L2
Lumen side
L1
TM1
TM6
TM3
TM5
B
TM9
TM10
TM2
TM8
A
TM7
TM4
C4
C1
C3
N-t
C2
Cytosol side
C-t
Side view
C
Core domain
Panel domain
C1
TM6
C4
L3
TM2
TM4
TM5
C3
TM9
B
A
TM3
N-t
C2
TM7
C-t
L5
L2
L1
TM8
TM10
L4
TM1
Top view (lumen side)

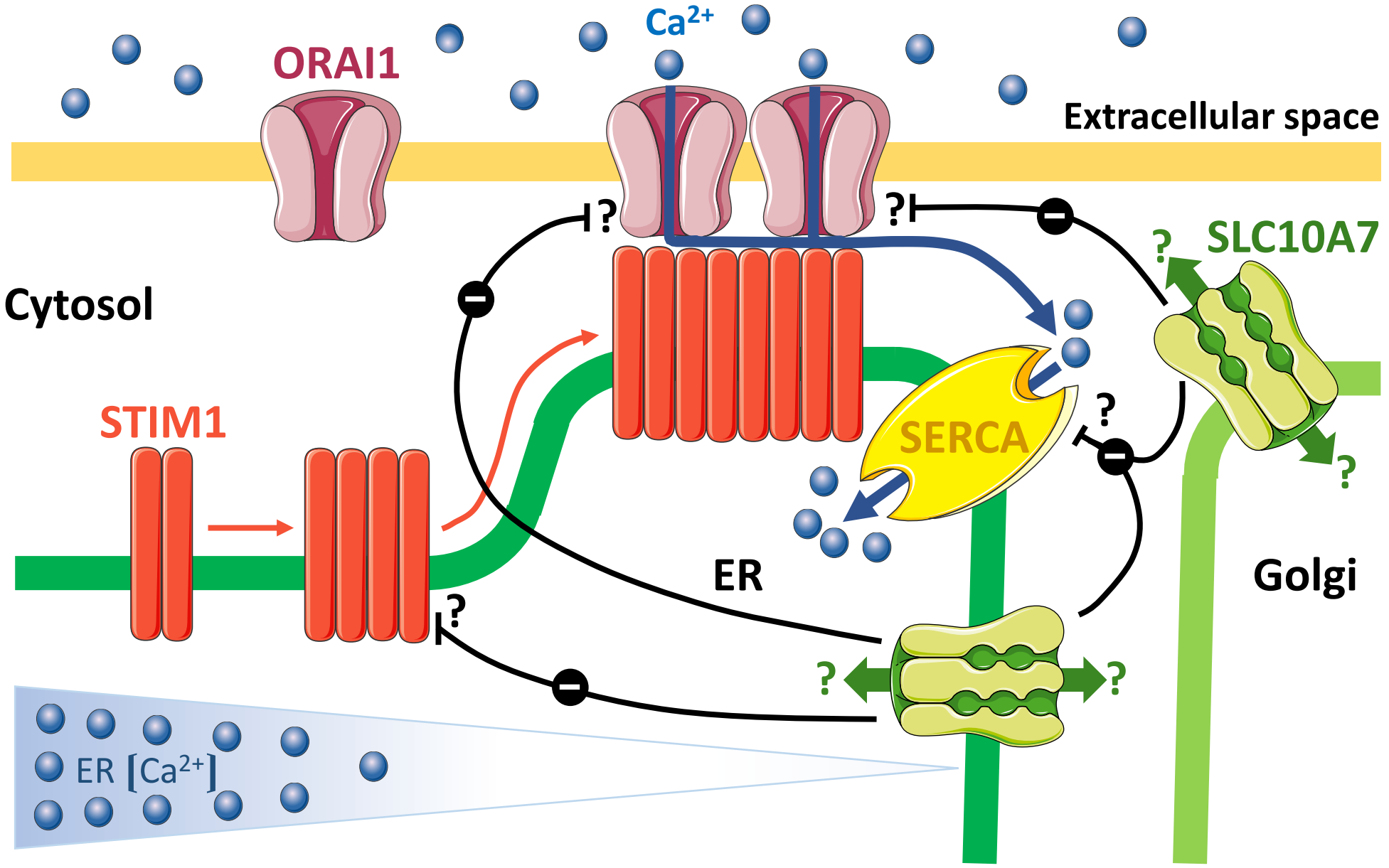
ORAI1
Ca2+
Extracellular space
Cytosol
STIM1
SERCA
SLC10A7
ER
Golgi
ER [Ca2+]

FIGURE 3

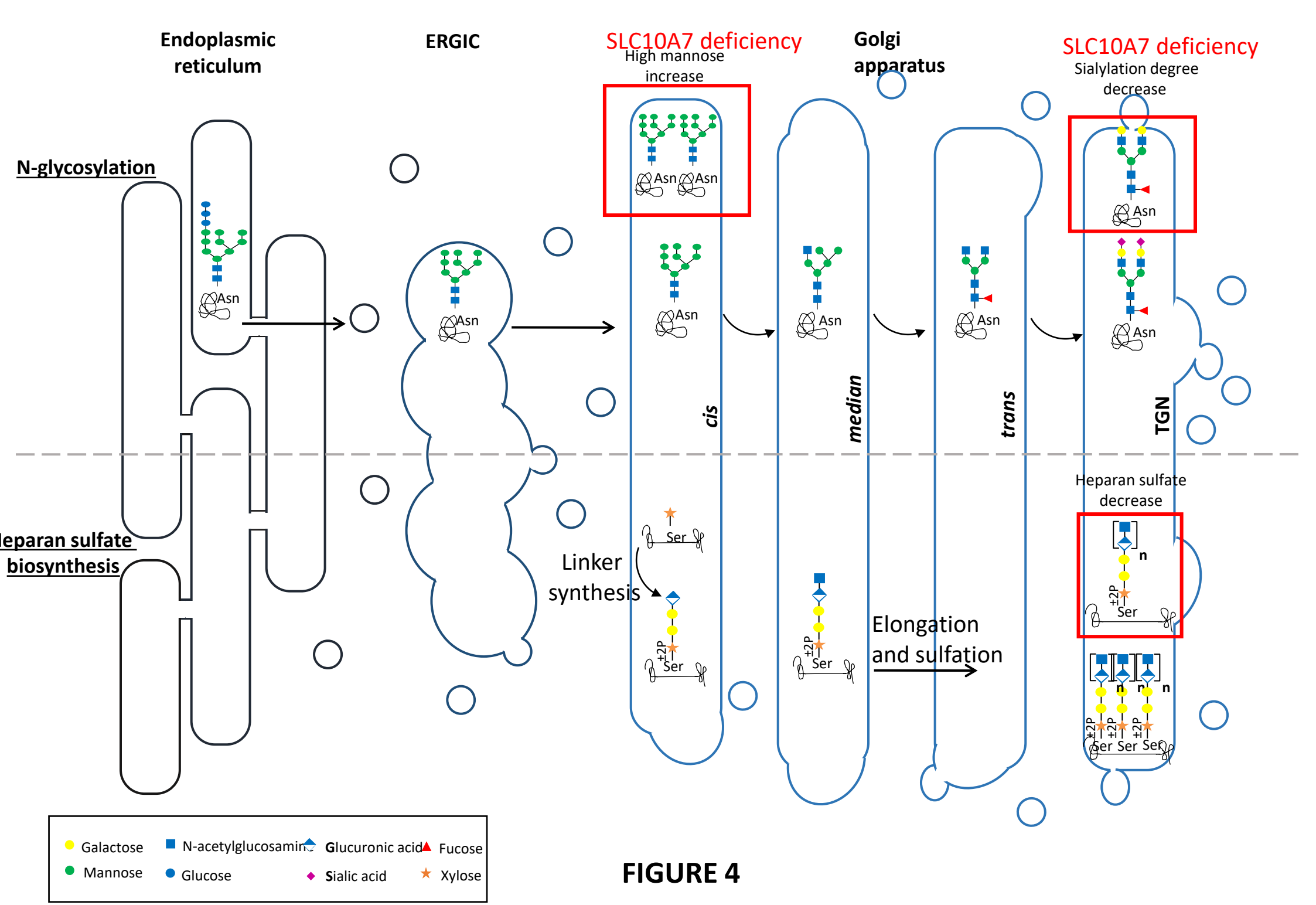
Endoplasmic reticulum
ERGIC
SLC10A7 deficiency
High mannose increase
Golgi apparatus
SLC10A7 deficiency
Sialylation degree decrease
N-glycosylation
Asn
cis
median
trans
TGN
Heparan sulfate biosynthesis
Linker synthesis
Ser
±2P
Elongation and sulfation
Heparan sulfate decrease
n
Galactose
N-acetylglucosamine
Glucuronic acid
Fucose
Mannose
Glucose
Sialic acid
Xylose

FIGURE 4